Electronic Supplementary Material (ESI) for Journal of Materials Chemistry A.

Supporting Information

Sandwich-like solid composite electrolytes employed as bifunctional separators for safe lithium metal batteries with excellent cycling performance

Kun Shi,*[ab] Zhengjie Xu,[a] Dawei Zheng,[a] Zeheng Yang,[a] and Weixin Zhang*[ab]

[a] *School of Chemistry and Chemical Engineering, Hefei University of Technology, Hefei, Anhui, 230009, China*
[b] *Institute of Energy, Hefei Comprehensive National Science Center, Hefei, Anhui, 230031, China*
E-mail: shikun@hfut.edu.cn (Kun Shi), wxzhang@hfut.edu.cn (Weixin Zhang)

Supplementary Figures S1-S10

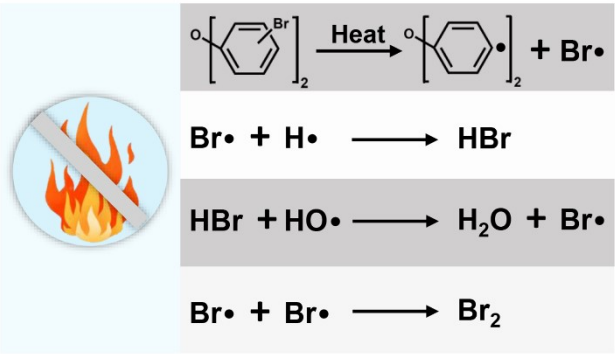

Fig. S1 The free radical elimination mechanism for good flame resistance of PVDF-DBDPO/PP separators.

The designed flame resistance of PVDF-DBDPO/PP separators is considered to come from a free radical elimination mechanism introduced by the incorporated DBDPO fillers (Fig. S1). For the electrolyte system using PVDF-DBDPO/PP separators, the PVDF chains, PP skeleton and limited organic solvent usually produce highly active OH• and H• when it starts burning, which can be instantly captured by the radical Br• generated from the incorporated DBDPO under heating, releasing the mixed gas composed of HBr, H_2O and Br_2 molecules, thereby the combustion chain reactions are blocked and self extinguishing occurs under the formed anoxic environment.[S1]

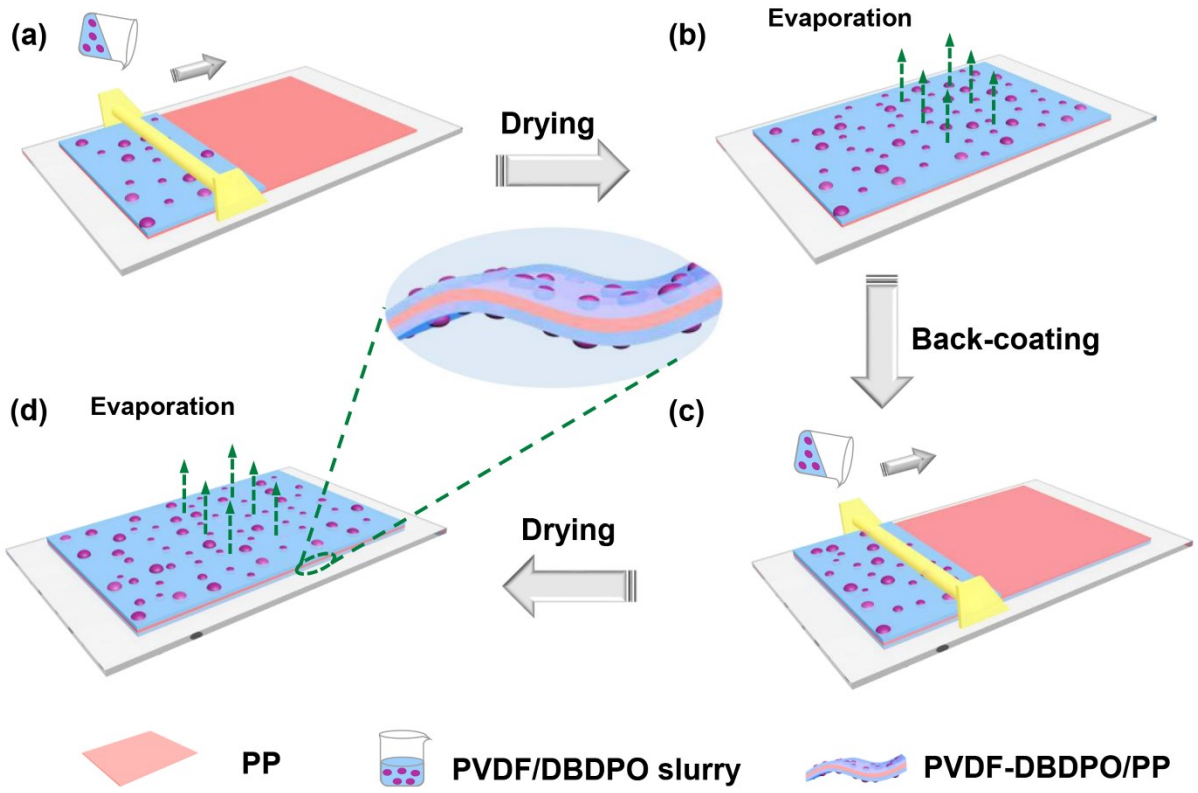

Fig. S2 The preparation process of PVDF-DBDPO/PP separator. (a) The first coating on one side of PP separator by PVDF/DBDPO slurry with (b) the following drying treatment, (c) the reverse coating on the other side of the pre-dried membrane, and (d) a drying treatment again for the final sandwich-like separator.

The PVDF-DBDPO/PP separators are prepared by a double-side coating technology according to our previous research (Fig. S2).[S2] Firstly, the PVDF-DBDPO slurry is preferentially cast on one side of the commercialized PP separator (Fig. S2a), with a following vaccum drying treatment at 60 ^{o}C for 5 h to obtain the pre-dried membrane (Fig. S2b). After that, a reverse coating is carried out using an equal amount of slurry (Fig. S2c), and the sandwich-like PVDF-DBDPO/PP separator can be finally obtained through another vaccum drying at 60 ^{o}C for 24 h (Fig. S2d).

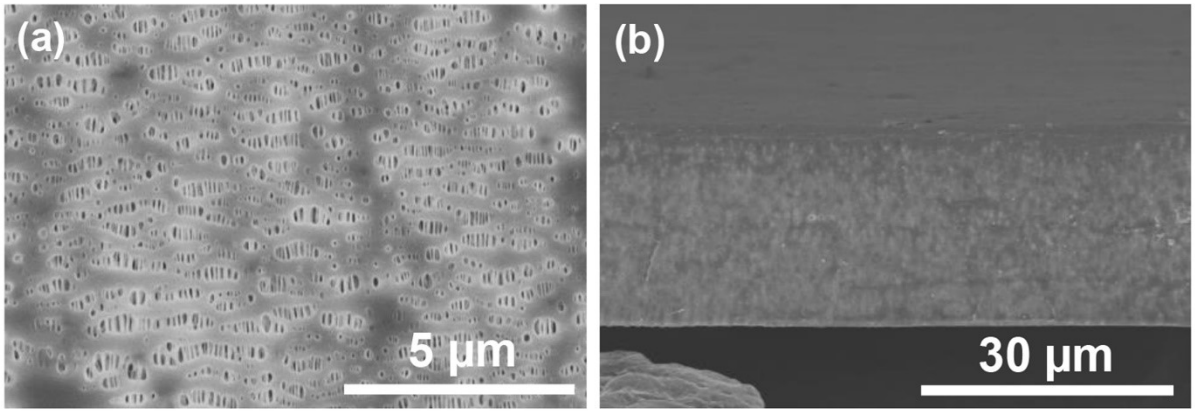

Fig. S3 The FESEM photographs of pristine PP separator. (a) The surface, and (b) cross section.

As shown in Fig. S3, large number of uniformly distributed nanopores can be clearly observed on not only the PP separator surface (Fig. S3a) but also its cross section (Fig. S3b), indicating a three-dimensional continuous nanopore network enabling electrolyte slurry infiltration during the preparation of PVDF-DBDPO/PP separators. Besides, the thickness of PP separator is measured as about 25 μm, consistent with the product identification.

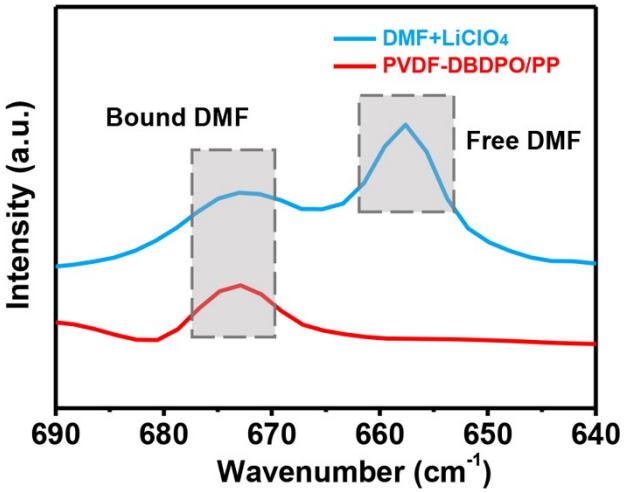

Fig. S4 FTIR spectra for DMF-$LiClO_4$ solution and PVDF-DBDPO/PP separator.

The molecule state of DMF in DMF-$LiClO_4$ solution (c_{Li}^+ = 1.0 M) and PVDF-DBDPO/PP separator are investigated by FTIR characterization (Fig. S4). The peak at 673 cm^{-1} usually represents the bound DMF existing in $[Li(DMF)_x]^+$ complexes, whereas that at 658 cm^{-1} indicates the O=C-N bending of free DMF molecules.[S3] Obviously, the DMF molecules in DMF-$LiClO_4$ solution coexist in the form of both free and bound state. But, only $[Li(DMF)_x]^+$ complexes can be found in the PVDF-DBDPO/PP separator, which is widely considered to be a clear signal of solid-state polymer electrolytes.[S4]

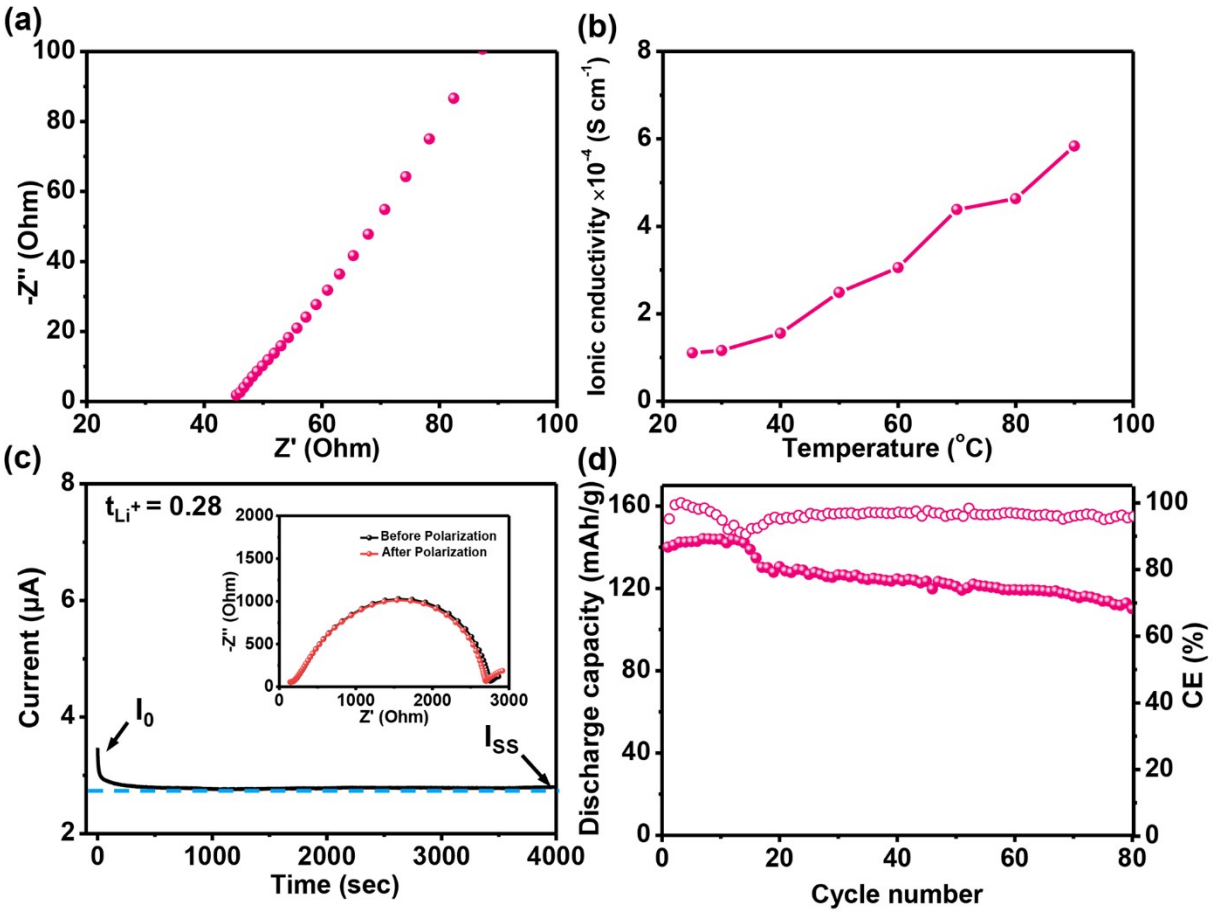

Fig. S5 Electrochemical properties of the liquid electrolyte-free solid-state PVDF-DBDPO/PP electrolyte. (a) EIS curve at 25 °C. (b) Ionic conductivities at the temperature from 25 to 90 °C. (c) DC polarization curve of the lithium symmetrical cell at 10 mV. (d) Cycling performance of the $LiFePO_4$/Li cells at 0.5 C under 25 °C.

As one kind of solid-state electrolyte, the liquid electrolyte-free PVDF-DBDPO/PP electrolyte itself can exhibit an ionic conductivity of 1.1×10^{-4} S cm^{-1} at 25 °C (Fig. S5a,b), and the acceptable lithium-ion transference number (0.28) implies a Li^+ migration behavior basically equal to that of the commercial liquid electrolyte (Fig. S5c). Besides, the $LiFePO_4$/Li cell with the solid-state PVDF-DBDPO/PP electrolyte delivers an initial specific capacity of about 140 mAh g^{-1}, with the capacity retention of 78.6% and the coulombic efficiency of 95.9% after 80 cycles at 0.5 C (Fig. S5d); which may be acceptable for the current room-temperature solid-state lithium metal batteries (LMBs), but still far below the performance level of general practical liquid-state LMBs. From this point of view, in order to take into account the battery safety and meanwhile the electrochemical properties, employing such solid-state PVDF-DBDPO/PP electrolyte as the separator loading with limited liquid electrolyte may actually be a compromise and quite effective solution at present.

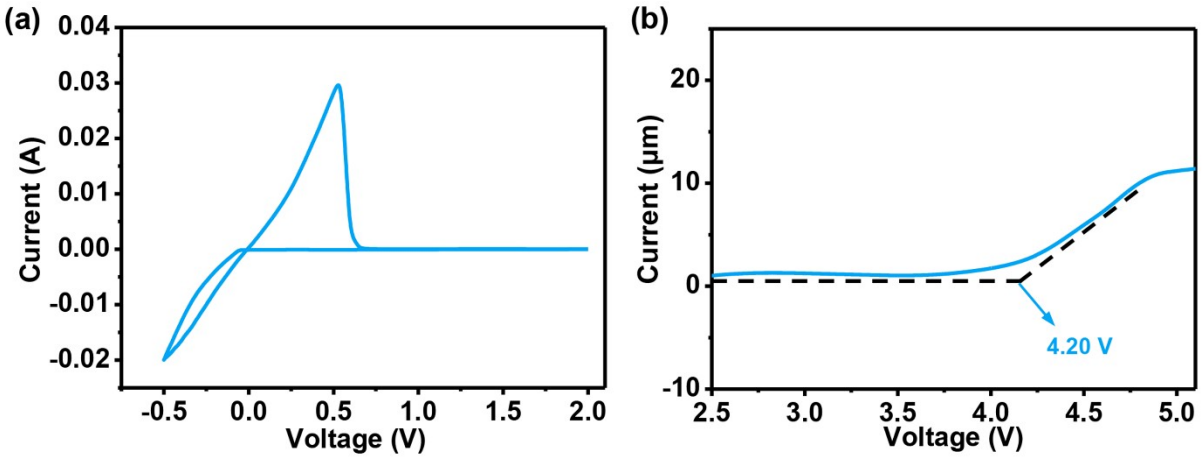

Fig. S6 (a) CV and (b) LSV curves of PP separator, at the scanning rate of 1 mV s^{-1}.

The CV result of PP separator shows the redox peaks below 0 V (*vs.* Li/Li^+), indicating a good reductive stability compatible with lithium metal (Fig. S6a).[S5] While the clear current rise appearing at about 4.2 V in the LSV curve (Fig. S6b), suggests the oxidation decomposition of the loaded liquid electrolyte.[S6]

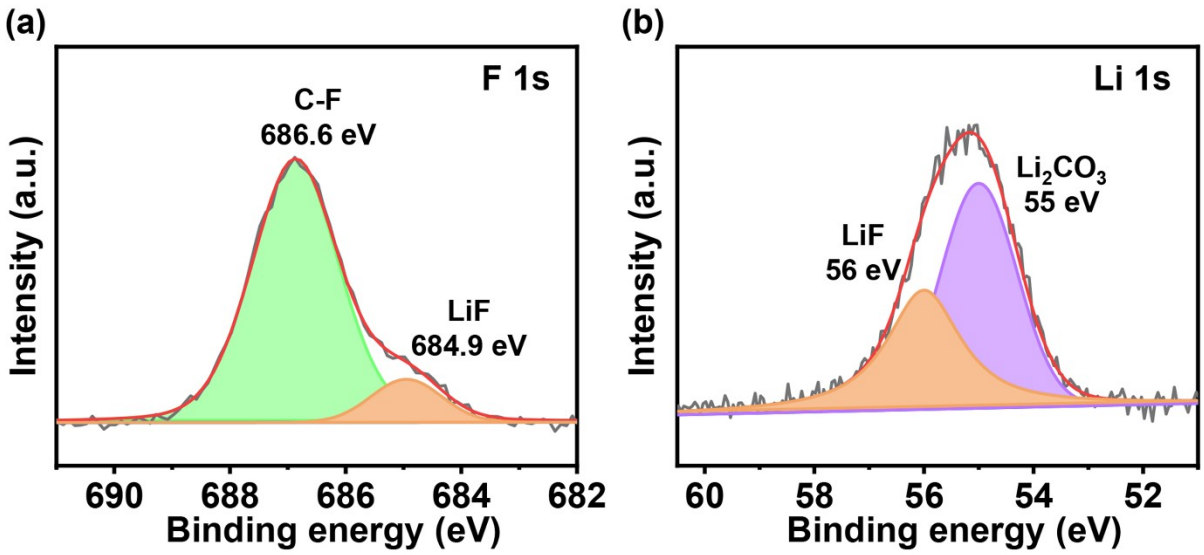

Fig. S7 X-ray photoelectron spectroscopy (XPS) spectra of the lithium anodes in Li|PVDF-DBDPO/PP|Li cell after 50 h cycling at 0.5 mA cm^{-2}. (a) F 1s and (b) Li 1s.

The chemical composition of the produced substance on the lithium metal surface is carefully analyzed by XPS (Fig. S7). The peaks at 684.9 eV corresponding to F 1s (Fig. S7a) and 56 eV belonging to Li 1s (Fig. S7b) confirm the existence of LiF, while the peak at 55 eV in the Li 1s spectrum indicates Li_2CO_3 (Fig. S7b), both of which are demonstrated as the main components of SEI film and beneficial to cell cycling stability.[S7]

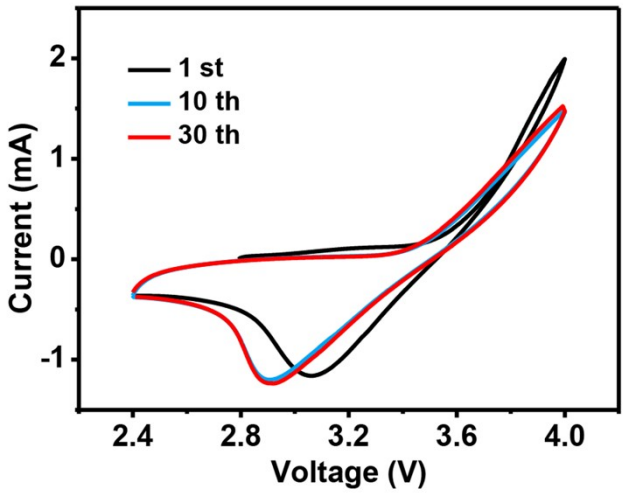

Fig. S8 Cyclic voltammetry (CV) curves for PVDF-DBDPO/PP separator with a scan rate of 10 mV s^{-1}.

The highly coincident CV curves of $LiFePO_4$|PVDF-DBDPO/PP|Li cell from the 10th to the 30th cycle indicate the excellent electrochemical stability of PVDF-DBDPO/PP separator during the charge-discharge operation between 2.4 to 4.0 V.

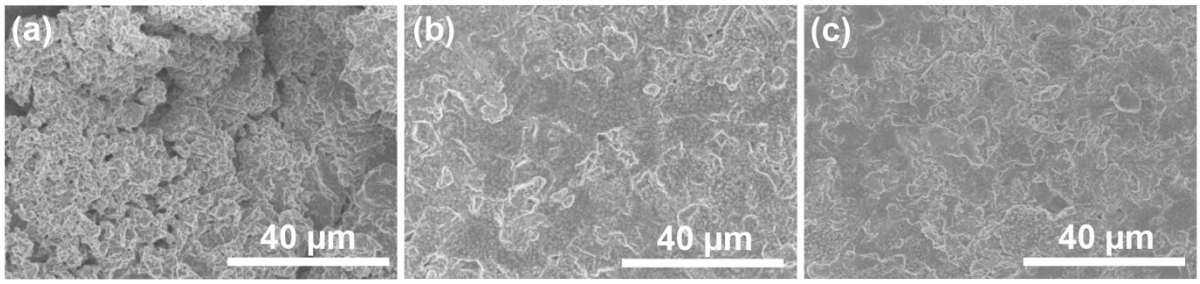

Fig. S9 SEM images of the lithium anodes after 1000 cycles for the $LiFePO_4$/Li cells with (a) PP, (b) PVDF/PP and (c) PVDF-DBDPO/PP separators, respectively.

Fig. S9 shows the surface morphology of lithium anodes in each $LiFePO_4$/Li cells after 1000 cycles at 0.5 C. For the $LiFePO_4$|PP|Li cell, there are massive lithium dendrites can be clearly found on the lithium metal surface (Fig. S9a). In contrast, the lithium anodes matched with the PVDF/PP and PVDF-DBDPO/PP separators deliver the relatively flat surface nearly without the acicular lithium dendrite formation (Fig. S9b,c). This result is believed to originate from the homogeneous Li^+ redistribution mechanism, which is beneficial for the smoother charge transfer as well as uniform lithium deposition, rather than the massive lithium dendrite generation caused by ion aggregations at the electrolyte/lithium anode interface.

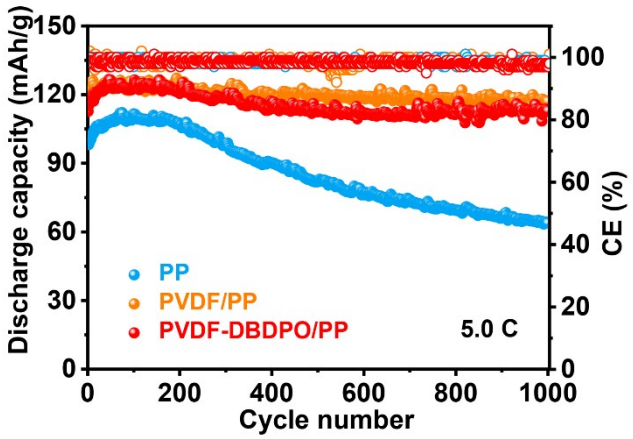

Fig. S10 Cycle performance of $LiFePO_4$/Li cells with PP, PVDF/PP and PVDF-DBDPO/PP separators at 5.0 C.

When operated at a high current density of 5.0 C (Fig. S10), the $LiFePO_4$/Li cell with PP separator only exhibit the initial discharge capacity of 98 mAh g^{-1}, which rapidly decays to 63 mAh g^{-1} with the capacity retention of 64.2% after 1000 cycles. Instead, the $LiFePO_4$|PVDF-DBDPO/PP|Li cell can demonstrate a significantly improved cyclic stability with a high initial discharge capacity of 113 mAh g^{-1} and barely decaying capacity after 1000 cycles.

References

[S1] Y. Cui, J. Y. Wan, Y. S. Ye, K. Liu, L. Y. Chou and Y. Cui, *Nano Lett.*, 2020, **20**, 1686-1692.

[S2] K. Shi, Z. J. Xu, M. Q. Huang, L. Zou, D. W. Zheng, Z. H. Yang and W. X. Zhang, *J. Membr. Sci*., 2021, **638**, 119713.

[S3] M. M. E. Jacob and A. K. Arof, *Electrochim. Acta*, 2000, **45**, 1701-1706.

[S4] X. Zhang, S. Wang, C. J. Xue, C. Z. Xin, Y. H. Lin, Y. Shen, L. L. Li and C. W. Nan, *Adv. Mater*., 2020, **32**, 2000026.

[S5] S. S. Zhang, Z. Li, Y. Guo, L. R. Cai, P. Manikandan, K. J. Zhao, Y. Li and V. G. Pol, *Chem. Eng. J*., 2020, **400**, 125996.

[S6] F. Q. Li, Y. Gong, G. F. Jia, Q. L. Wang, Z. J. Peng, W. Fan and B. Bai, *J. Power Sources*, 2015, **295**, 47-54.

[S7] X. Q. Zhang, X. B. Cheng, X. Chen, C. Yan and Q. Zhang, *Adv. Funct. Mater*., 2017, **27**, 1605989.